Received 11 November 2021; revised 22 December 2021; accepted 4 January 2022.
Date of publication 10 January 2022; date of current version 28 January 2022.

Digital Object Identifier 10.1109/OJUFFC.2022.3141333

Multipath Flow Metering of High-Velocity Gas Using Ultrasonic Phased-Arrays

CHRISTOPH HAUGWITZ[1] (Student Member, IEEE), CLAAS HARTMANN[1] (Graduate Student Member, IEEE), GIANNI ALLEVATO[1] (Student Member, IEEE), MATTHIAS RUTSCH[1] (Graduate Student Member, IEEE), JAN HINRICHS[1] (Graduate Student Member, IEEE), JOHANNES BRÖTZ[2], DIETER BOTHE[3], PETER F. PELZ[2], AND MARIO KUPNIK[1] (Senior Member, IEEE)

[1]Measurement and Sensor Technology Group, Technische Universität Darmstadt, 64289 Darmstadt, Germany
[2]Chair of Fluid Systems, Technische Universität Darmstadt, 64289 Darmstadt, Germany
[3]Mathematical Modeling and Analysis Group, Technische Universität Darmstadt, 64289 Darmstadt, Germany
CORRESPONDING AUTHOR: C. HAUGWITZ (christoph.haugwitz@tu-darmstadt.de)

This article has supplementary downloadable material available at https://doi.org/10.1109/OJUFFC.2022.3141333, provided by the authors.

ABSTRACT In this work we combine a multipath ultrasonic gas flow meter (UFM) with an ultrasonic air-coupled phased-array. This allows complementing the advantages of a multipath UFM, i.e. higher accuracy and more robustness to irregular flow, with the extended velocity measuring range due to sound drift compensation via a phased-array. We created a 3D-printed flow meter consisting of an 8×8 $\lambda/2$ phased-array for transmission and 14 individual receivers for seven upstream and seven downstream sound paths. Measurements were conducted in a test rig with a maximum gas flow rates of $8.3\,\mathrm{m^3\,s^{-1}}$ ($107\,\mathrm{m\,s^{-1}}$). A differential pressure nozzle was used as reference sensor. Three configurations were compared: Parallel sound paths with a single transmitter; parallel sound paths with the phased-array as transmitter; and fan-shaped sound paths with the phased-array as transmitter. The signal-to-noise ratio (SNR) and deviation of measured flow were used as comparison criteria. In addition, we measured the optimum steering angles of the phased-array required to compensate the sound drift effect. Using the phased-array with the sound drift effect compensation enabled and disabled, the SNR increases by 10.6 dB and 4.95 dB, respectively, compared to the single transmitter setup at $83\,\mathrm{m\,s^{-1}}$. Furthermore, the phased-array with compensation active, extends the velocity measuring range by 29%, from $83\,\mathrm{m\,s^{-1}}$ to $107\,\mathrm{m\,s^{-1}}$, while maintaining a similar standard deviation of the flow measured. Besides demonstrating that a phased-array in a gas flow meter significantly extends the measurement range, our setup qualifies as versatile research platform for designing future high-velocity gas flow meters.

INDEX TERMS Ultrasonic phased-array, gas flow metering, multipath ultrasonic flow-meter, sound drift effect.

I. INTRODUCTION

ULTRASONIC flow meters (UFMs) are widely used in industrial applications [1]. Most commonly, the transit time method is used because of its high accuracy and absence of moving parts [2].

Using the transit time method, the average flow velocity across a sound path v_{av} is calculated using the upstream t_{up} and downstream t_{down} propagation times, the path length L, measured from the receiver to the transmitter, and its inclination angle α [Fig. 1(a)], [3], [4], i.e.

$$v_{\mathrm{av}} = \frac{L}{2\sin(\alpha)}\left(\frac{1}{t_{\mathrm{down}}} - \frac{1}{t_{\mathrm{up}}}\right). \tag{1}$$

However, there is a significant difference between the calculated average flow velocity across a sound path v_{av} and the desired flow velocity averaged over the pipe area v_{area}, due to the lower flow velocities near the walls. In order to obtain the desired velocity v_{area} in a single path UFM, an in-line calibration is required to provide the meter factor k [1].

In contrast to a single path UFM, multipath UFMs measure the flow at different sound path locations and do not require an in-line calibration. Additionally, the accuracy of the flow meter and its tolerance against irregular flow profiles is increased [5]. While different multipath arrangements are possible, e.g. fan-shaped [6], isosceles triangular [7], orthogonal or star shaped arrangement [8], the parallel arrangement of the paths [Fig. 2(a)] is most commonly used [8].

In a multipath UFM, the resulting flow velocity v_{area} is calculated by integrating the flow velocity profile $v(y, z)$ over two-dimensional sections. The sound propagation already

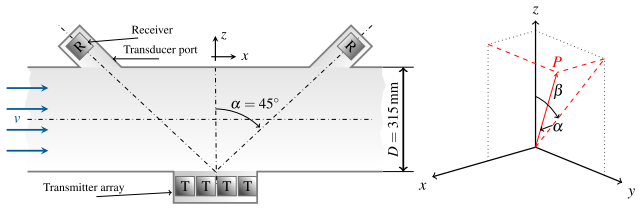

FIGURE 1. The measuring pipe consists of multiple transmitters (T) forming a phased-array for steering its sound beam to target the receivers (R), and compensate the sound drift effect. There are seven receivers for the upstream and downstream path each, not shown in the figure. The gas flow is indicated by the arrows on the left side. The origin of the coordinate system in this work is in the center of the phased-array, which is placed on the *x*-*y*-plane and is orthogonal to the *z*-axis (b). The gas flows in positive *x* direction.

integrates the flow velocity across the z direction [Fig. 1(b)], reducing the integration problem by one dimension. The flow velocity profile projection onto that single dimension is called flow-area function $F(y)$ [9]. The flow-area function $F(y)$ is only measurable at the discrete positions of the paths y_i [Fig. 2 (a)] using the average flow velocities across each path $v_{\mathrm{av},\,i}$, the path lengths L_i, and the inclination angles α_i, i.e.

$$F(y_i) = v_{\mathrm{av},\,i}\, L_i\, \cos(\alpha_i). \tag{2}$$

Ideally, the desired flow velocity v_{area} can be calculated as an integral across the flow-area function $F(y)$. However, the integral must be approximated as a weighted sum, since only a finite number of paths is available [9], i.e.

$$v_{\mathrm{area}} = \int_{-R}^{R} F(y)dy \approx \sum_{i=1}^{N} w_{\mathrm{i}}\, v_{\mathrm{av},\,i}. \tag{3}$$

The choice of the ideal weights w_{i} and path positions y_i is a standard quadrature problem.

There are four common quadrature methods: Gauss-Legendre, Tchebychev, Optimally Weighted Integration for Circular Sections [10], and Tailored [11], [12]. These methods are compared in [5], [9], [13]–[15] with different conclusions, dependent on the profile used. This work uses the Tchebychev method, due to its closed-form solution.

There are other methods to calculate the velocity v_{area} from the measured velocities v_{av}, which require an exact prior knowledge of the pipe configuration and, therefore, of the flow profile [16]–[19]. These methods lead to a highly increased accuracy only if the specific prior knowledge of the flow profile is applicable.

Multipath UFMs have higher accuracy and more robustness to irregular flow distributions. However, the parasitic sound drift effect limits the range of measurable flow rates. The sound drift effect is the shift of the sound intensity, due to the flow velocity, decreasing the noise ratio (SNR). One option to increase the range of measurable flow rates is to use broadband transducers and a sophisticated signal processing algorithm in order to raise the SNR, e.g. [20]–[22]. Another option is to shrink the transducer aperture in order to get a wider beam width, which reduces the sound drift effect. Both options reduce the sound pressure level of the transducers. However, a third option is to compensate the sound drift effect mechanically, which includes shifting the transducers [23] or rotating the transducers [24]. This comes at the downside of the UFM becoming asymetric. Using a phased-array to compensate the sound drift effect has the ability to steer the compensation angle without mechanically changing the setup. By compensating the sound drift effect, the range of measurable flow rates can be extended.

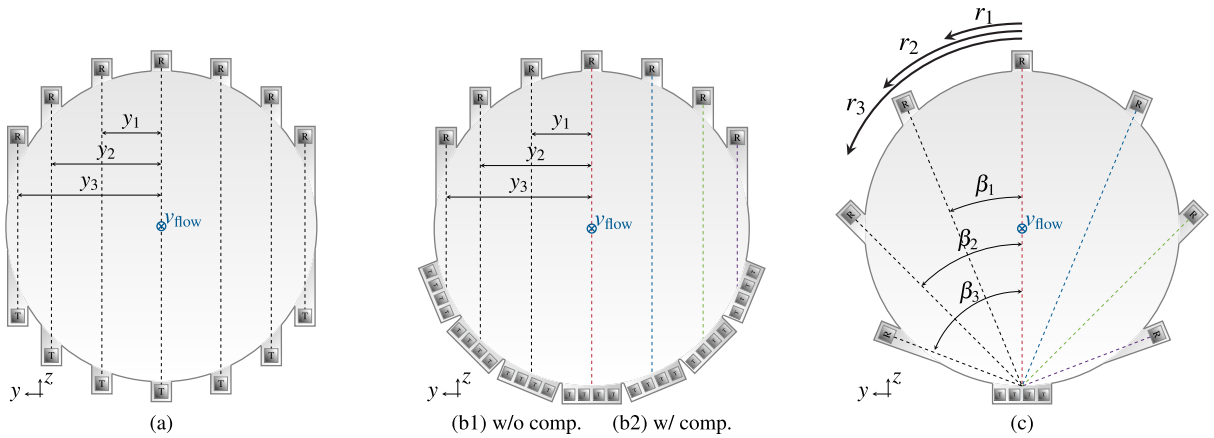

FIGURE 2. In this work, three different possibilities (b1, b2, c) of using a phased-array in a multipath UFM are evaluated and compared to a reference multipath UFM with single transducers (a). The UFMs are cut on the plane $x + z = 0$ and viewed from aside. In (b), the single transducers from the reference UFM are replaced with phased-arrays in order to increase SNR and to be capable of sound drift compensation. This layout is examined with and without compensation of the sound drift effect. In (c), the sound paths are arranged in a fan-shaped path arrangement, in order to require only one phased-array while maintaining the increased SNR and the capability of sound drift compensation. This layout is examined with compensation enabled.

A phased-array consists of multiple, specifically arranged transducers. If all transducers are used for transmission, the interference of the sound waves will create a directional radiation pattern, consisting of one high-intensity main lobe and several side lobes for a half wavelength maximum inter-element spacing $d = \lambda/2$. The direction of the main lobe is steerable using time-delayed transducer driving signals, also called beamforming.

Ultrasonic phased-arrays have been used in various ways for flow metering. The basic idea of using phase-shifted transmitter or receiver signals in a flow meter has been initially patented by Lowell [25]. Hall [26] transmits a pulse to a reflector and estimates the direction of arrival of the reflection. Then, the flow velocity is calculated based on the angle of arrival. Kang *et al.* [27] use each single transducer in an array for transmitting to a common receiver. Using this spatial averaging technique, they generate as many acoustic paths as there are transducers in the array, which are then averaged.

In this work, an air-coupled ultrasonic phased-array [28] with an inter-element spacing of $d = \lambda/2$ is used to transmit grating-lobe-free beamformed sound burst to different receivers, while compensating for the parasitic sound drift effect. The compensation of the sound drift effect using a phased-array has been proposed for liquids by Dassler [29], and for gases by Kang *et al.* [30] and in our previous work [31]. In [30] and [31] various manufactured phased-arrays were tested on single path arrangements in gas flow meters with flow rates up to $0.694\,\mathrm{m^3\,s^{-1}}$ ($41.5\,\mathrm{m\,s^{-1}}$). In [32], we experimentally prove the resulting extension of the velocity measuring range up to $7.8\,\mathrm{m^3\,s^{-1}}$ ($100\,\mathrm{m\,s^{-1}}$) using this technique on single path arrangements in gas UFMs.

In this work, we examine whether and to what extent using a phased-array in a gas flow measurement setup will extend the measuring range by increasing the SNR via sound drift effect compensation with the addition of multipath support, based on our previous work [32]. This allows us to introduce a versatile setup, that acts as a research platform, capable to support the design of future UFMs with optimum inclination angles for specific velocity ranges up to $107\,\mathrm{m\,s^{-1}}$.

This paper is structured as follows: At first, the flow rig to test the constructed UFM (Section II-A) and the mechanical setup of the UFM in the proposed layout (Section II-B) are described. Next, the transducers used (Section II-C) are shown, followed by the analysis of optimum steering angle, transit time, and received amplitudes (Section II-D). Then the measurement results are presented and discussed (Section III).

II. METHODOLOGY

We will examine three different configurations of a multipath UFM using phased-arrays in a test flow rig, and compare them to our reference UFM, which is a parallel path single transmitter multipath UFM [Fig. 2(a)]. The reference UFM is designed to be as close as possible to the phased-array UFM, in order to ensure comparability. First, the parallel path setup with multiple phased-arrays as transmitters is examined [Fig. 2(b1)], without using the ability of the phased-array to dynamically compensate the sound drift effect. Second, the same setup is used, but with the compensation of the sound drift effect enabled, in order to investigate the effect of the sound drift compensation [Fig. 2(b2)]. Third, the fan-shaped path setup [Fig. 2(c)] is examined, as this is a cost-effective option with a single phased-array as transmitter required. In order to optimize the construction effort, all these UFM types are integrated in a single 3D-printed pipe. The parallel path arrangement with multiple phased-arrays is imitated sequentially using the fan-shaped path arrangement with only a single phased-array. At first, the measurement along the red path is conducted. Then, the fan-shaped arrangement [Fig. 2(c)] is rotated counterclockwise (r_1) around the x-axis by β_1. Now, the measurement is conducted along the blue path, which is then equal to the blue path in the parallel path arrangement [Fig. 2(b)]. This procedure is repeated for the green path (r_2, β_2) and the purple path (r_3, β_3).

A. SETUP OF THE FLOW RIG

We analyze our UFM using a test flow rig capable of providing a volumetric airflow of $8.3\,\mathrm{m^3\,s^{-1}}$ ($107\,\mathrm{m\,s^{-1}}$), which is build according to ISO 5801:2017(E) [33]. The airflow is kept constant during the measurement, with its variation being below the accuracy of the reference meter. As reference meter, the volumetric flow rate is measured with the differential pressure method across a calibrated ISA-1932 type nozzle (DIN EN ISO 5167-3 [34]). The flow rig is described in more detail in [32]. Environmental measurements required for the flow calculation are conducted with a combined temperature, pressure and humidity sensor BME280 (Bosch, Stuttgart, Germany).

B. MECHANICAL DESIGN OF THE UFM SETUP

In this section, the mechanical setup of the multipath UFM with phased-array as transmitter [Fig. 2(c)] is described at first. The pipe construction is outlined and the receiver positions are derived. At last, we specify how we use this constructed UFM to measure in a parallel path arrangement either with phased-arrays as transmitters, or with single transmitters instead.

The pipe of the UFM has an inner diameter of 315 mm and is 3D-printed using a Fused Deposition Modelling (FDM) [35] 3D-printer (CR-10S5, Creality 3D) [Fig. 3(c)]. The pipe is printed in two halves and bonded with adhesive. On top of the pipe is space for the ultrasonic phased-array [Fig. 3(a)].

In our fan-shaped setup, the acoustic paths are arranged according to a transformation from parallel paths to fan-shaped paths of the Tchebychev method. The Tchebychev method provides closed form solutions for the positions of the paths $\frac{y_i}{R} = \cos[\pi i/(N+1)]$ and the weights $w_{i,\mathrm{TC}} = \pi/(N+1)\sin[\pi i/(N+1)]$, and does not use any assumption on the flow. The volumetric flow Q_{meas} can be calculated with a weighted sum of the measured velocities using the radius of the pipe R, the number of paths N, the

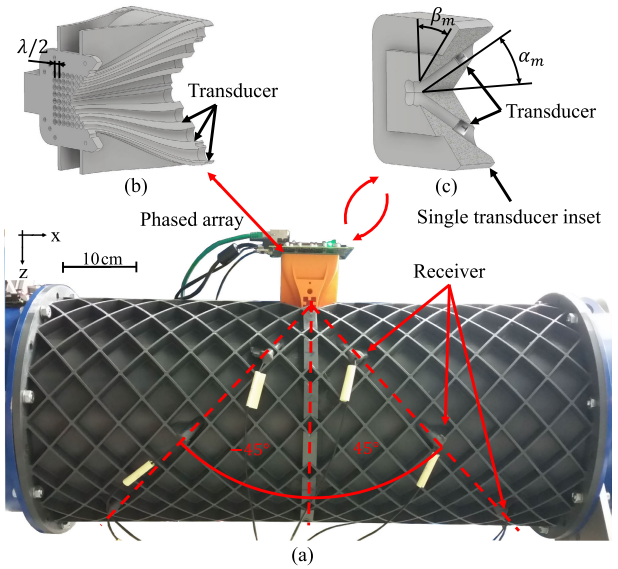

FIGURE 3. The UFM consists of a 3D-printed pipe with seven receivers for the upstream and downstream path each (a). On top, there is the transmitting phased-array with its 3D-printed waveguide (b). The phased-array mounting can be detached and replaced with various 3D-printed mountings holding two single transducers, which point to specific receivers (c). The complete pipe can be mechanically rotated around the *x*-axis in steps of 22.5° for sequentially imitating a parallel path ultrasonic flow meter with either a phased-array or single transducer as transmitter.

measured velocities $v_{\mathrm{av,i}}$, the lengths of the paths L_i, and the inclination angle α_i [9], i.e.

$$Q_{\mathrm{meas}} = R \sum_{i=1}^{N} w_{i,\,\mathrm{TC}}\, v_{\mathrm{av,i}}\, L_i\, \cos(\alpha_i). \tag{4}$$

Since the Tchebychev method only features parallel paths, a transformation from the positions of the parallel paths y_i to the angles between the fan-shaped paths β_i is required. With this transformation the path lengths remain equal to the parallel path arrangement, i.e.

$$\beta_i = \arcsin\left(\frac{y_i}{R}\right). \tag{5}$$

This transformation in 3D is known as rebinning in computer tomography [36], [37]. With the Tchebychev arrangement method, the angles β_i are exact linearly dependent on the path index i, i.e.

$$\beta_i = \left(1 - \frac{2i}{N+1}\right)\frac{\pi}{2} \quad \text{for } i \in \{1, 2, \ldots, N\}. \tag{6}$$

Here, N is the number of paths, for which we chose $N = 7$.

The receivers in each upstream and downstream direction are positioned all on the same plane $x - |z| = 0$ for $z \in [0, D]$ and $y \in [-\frac{D}{2}, \frac{D}{2}]$, leading to different inclination angles $\alpha_i = \arctan(\cos\beta_i)$ on each path. Therefore, the angles of the ultrasonic paths are $(\alpha_{\mathrm{m}}, \beta_{\mathrm{m}}) = \{(20.94°, 67.5°), (35.26°, 45°), (42.73°, 22.5°), (45°, 0°)\}$ and the corresponding mirrored angles.

The UFM in the parallel path arrangement [Fig. 2(b)] is sequentially imitated from the layout in the fan-shaped path arrangement [Fig. 2(c)]. This is done by mechanically rotating the UFM by the angle β_i around the flow axis. Each time the fan-shaped arrangement is rotated by β_i, one path is vertical, and, along that path, the measurement is conducted. After all the path velocities v_{av} are measured, they are combined to imitate a parallel path UFM. The flow rig pipes can only be turned discretely in steps of 22.5°, which is the rationale to choose the aforementioned $N = 7$ sound paths. Due to the radially symmetric flow profile in the test rig [38], the flow measurements will be symmetric. Therefore, the pipe only is mechanically turned to four directions instead of seven.

In order to provide a reference for these two phased-array setups, we additionally require a single transmitter multipath UFM. Therefore, the phased-array inset can be replaced with one of four 3D-printed mountings pointing in the four directions of the receivers into which the two single transducers are inserted [Fig. 3(b)].

The UFM design presented is a nonreciprocal UFM, since a flow measurement is conducted with two different receivers each for the upstream path and the downstream path [Fig. 1(a)]. UFMs which compensate the sound drift effect mechanically are usually nonreciprocal [24], [39], which leads to a small offset error at zero flow [40]. However, as the aim is to measure flow at high velocities, this error is acceptable, as it is below other sources of error. The reference method with single transducers is also built as nonreciprocal UFM for comparison purposes.

C. TRANSDUCER IN THE UFM SETUP

The transducers used for the phased-array and also for the single transmission are efficient, low-cost, narrow-band, air-coupled transducers of type MA40S4S (Murata Manufacturing Co., Nagaokakyo, Japan) with a resonance frequency of 40 kHz and a diameter of $d_t = 10$ mm. The receivers are of type MA40S4R (Murata).

The ultrasonic phased-array has an 8×8 uniform rectangular arrangement with a 3D-printed waveguide [Fig. 3(a)] to reduce the effective inter-element spacing from d_t to $d_w = 4.3\,\mathrm{mm} \approx \lambda/2$ for grating lobe free beamforming [28]. The different lengths of the waveguide are compensated by delaying the signal of the corresponding transducer m by $\Delta t_{w,m}$ [41]. In order to steer the sound beam to a given angle (α_s, β_s), the time delay of the m-th transducer $\Delta t_{s,m}$ is

$$\Delta t_{s,m} = \left[x_m \sin(\alpha_s) + y_m \sin(\beta_s)\cos(\alpha_s)\right]/c + \Delta t_{w,m}, \tag{7}$$

where (x_m, y_m) are the coordinates of the m-th transducer. The impact of the waveguide on the sound pressure field of the array was examined in previous work [41], [42].

We use identical transceiver electronics for all of the 14 receivers, the phased-array, and the single transmitters. The signals are sampled with a rate of 195 kSa s^{-1}. The data is sent to a PC via Ethernet. The electronics and the waveguide have been utilized for 3D imaging in [42], where they are described in more detail.

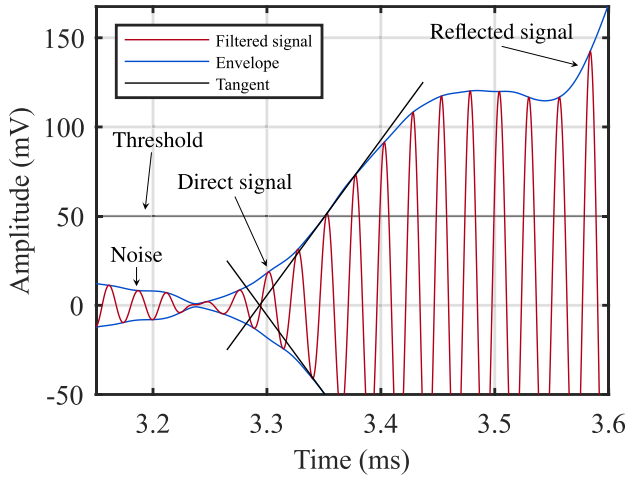

FIGURE 4. **A worst case signal received consists of a small amplitude direct signal and higher amplitude reflected signal. The signal is filtered (red) and the envelope is extracted (blue). The transit-time is extracted using a threshold-tangent intersection approach (black). The amplitude is defined as the RMS value of the first three cycles after the tangent intersection. These algorithms have been selected to cope with the changing signal shape at varying steering angles and to evaluate only the first incoming signal.**

D. ANALYSIS OF OPTIMUM STEERING ANGLE, TRANSIT TIME, AND RECEIVED AMPLITUDE

The aim of the data evaluation is to obtain the following three parameters for each flow rate. First, the ideal compensation angle, which is the steering angle of the phased-array in order to receive a maximum amplitude. Second, the overall received amplitude is evaluated. Third, the overall transit time is evaluated, that is used to calculate the flow velocity.

In order to determine the ideal angle for sound drift compensation for each flow rate, first, we define a grid of possible discrete angles in steps of 3°, i.e. $\alpha \in \{-84°, -81°, \ldots, 69°\}$ and $\beta \in \{-85.5°, -82.5°, \ldots, 85.5°\}$. The phased-array sends a beamformed five-cycle burst of $V_{pp} = 20\,\text{V}$ at $f = 40\,\text{kHz}$ to each angle on the grid, while all receivers are recording the signals. This processs takes 20 ms on our hardware. This is repeated 25 times and the signals are averaged. The averaged received signals are then upsampled and filtered.

We define the received amplitude as the RMS value of the first three cycles, as there are additional acoustic reflections arriving shortly after the direct signal (Fig. 4). They occur especially when the main lobe is steered to the wall, so that the sound reflects to the receiver, or when the main lobe is steered to the opposite direction, due to side lobe reflections. Since the phased-array searches for an optimum angle, it tries every angle and, therefore, also these critical angles at, e.g. $\beta = 45°$ or the depicted angle at $(\alpha, \beta) = (-66°, 0°)$ which is recorded with the upstream center receiver (Fig. 4). In this case, the received signal is the superposition of a low-amplitude direct signal from a side lobe of the phased-array and a high-amplitude delayed signal, due to the longer reflection path. The received amplitudes for each transmission direction are smoothed with a 2D Gaussian filter with $\sigma = 10°$, in order to filter out ripples (Fig. 5). The optimal compensation angle corresponds to the maximum of this smoothed amplitudes.

Second, we define the overall received amplitude as the received maximum amplitude at the ideal compensation angle. If the sound drift compensation is inactive, the overall received amplitude will be obtained from the received amplitude at the receiver direction (Fig. 5). The overall received

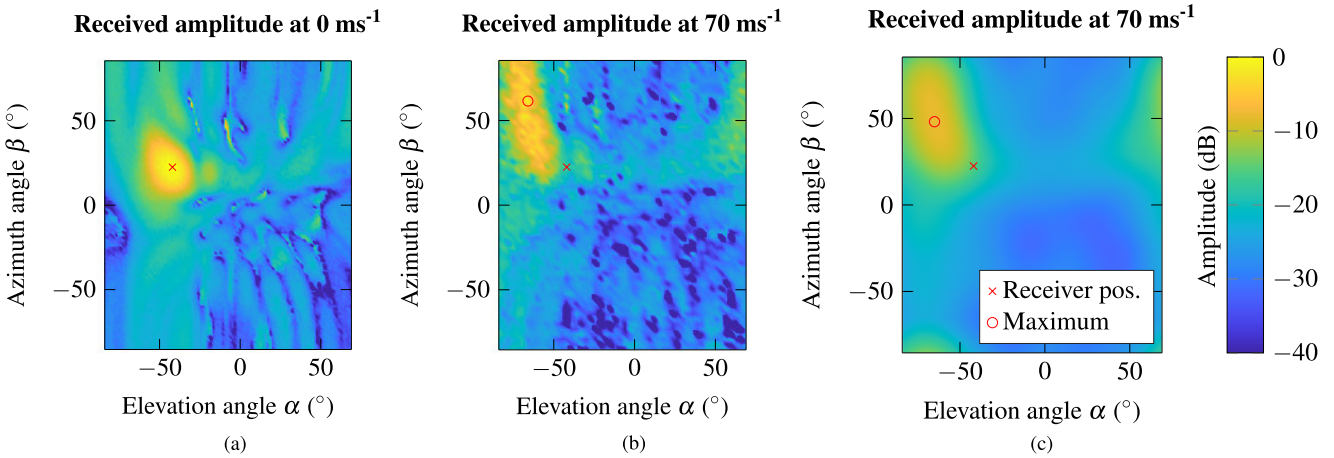

FIGURE 5. **The phased-array steers to α and β directions in 3° increments in both dimensions. At each increment a burst is sent which is received by the single transducers and evaluated for its amplitude. With zero flow, the receiver at $\beta = 22.5°$ (x) receives the maximum amplitude, when the phased-array is steered to its direction (a). The features next to the main beam are caused by the directivity pattern of the phased-array in the first few periods of the sound burst. When the air velocity is 70 ms^{-1}, the phased-array must steer to a different angle to receive the maximum amplitude (b). Due to the flow, the received amplitude is scattered and the maximum received amplitude (o) includes noise. In order to address this problem, a Gauss-filter is applied for smoothing (c). The position of the maximum smoothed received amplitude is used as the ideal compensation angle.**

amplitude s and the root mean square (RMS) noise amplitude n, measured in a 1 ms interval before each pulse transmission are used for SNR evaluation, i.e

$$\mathrm{SNR} = 10 \cdot \log\left(\frac{s^2}{n^2}\right). \tag{8}$$

Third, the transit time evaluation algorithm is based on the envelope of the averaged received signal, as proposed by Mu *et al.* [43]. The threshold detection on the envelope of the averaged received signal is performed in a single expectation window calculated in advance, based on the possible propagation times, in order to reduce the computation time. The zero-crossing of the tangent at the threshold is used to estimate the transit time of the signal, resulting in similar transit times for varying amplitudes of the incoming signal (Fig. 4). This gives good results for our data. The aim of this transit time evaluation method is to evaluate only the first, direct signal, and not the reflections. In order to reduce inaccuracies, all measured transit times in a small area with a radius of 5° surrounding the optimal compensation angle are averaged to obtain the overall transit time. If the sound drift compensation is inactive, we use the measured transit times in a circle with the same 5° radius surrounding the receivers direction.

Dead times t_{dead} to compensate for geometry and beamforming delays are subtracted from the overall transit time so that the resulting compensated transit-time corresponds to the sound path in the pipe, that is

$$t_{\mathrm{dead}} = t_{\mathrm{d,wg}} + t_{\mathrm{d,rp}} + t_{\mathrm{d,ar}}. \tag{9}$$

The time $t_{\mathrm{d,wg}}$ is the propagation delay due to the waveguide, $t_{\mathrm{d,rp}}$ is the propagation delay due to the receiver pocket, and $t_{\mathrm{d,ar}}$ is the beamforming delay calculated from the width of the array d_{array}, the steering angles α and β and the temperature dependent speed of sound c, i.e.

$$t_{\mathrm{d,ar}} = \frac{d_{\mathrm{array}}}{2c}\left(\sin(\alpha) + \sin(\beta)\cos(\alpha)\right). \tag{10}$$

The compensated transit time with zero flow is used to calibrate for offset errors due to the nonreciprocity of the UFM. The offset error is different for each path and around $\pm 10\,\mu$s.

The flow velocity of each path [Eq. (1)] and the volumetric flow [Eq. (4)] is evaluated from the compensated transit times. Two comparison parameters are calculated from all measured volumetric flow rates. First, the standard deviation of the volumetric flow values is estimated using the empiric standard deviation from all transit-time measurement in the area surrounding the target angle. Second, the average flow error is calculated as the difference of the mean measured flow rates and the reference flow normalized to the end value.

III. RESULTS AND DISCUSSION

A. MEASURED IDEAL COMPENSATION ANGLE

The compensation angles are measured at each flow rate by scanning every angle and denoting the maximum received amplitude. In order to compensate the sound drift effect, the phased-array has to steer in $-x$ direction, against the flow, as expected (Fig. 6). Additionally, the phased-array steers orthogonal to the flow. For the upstream direction, it steers outwards and for the downstream direction, it steers inwards. This is due to sound refracting orthogonal to the flow, in the direction of the flow profile gradient [44].

In order to validate the compensation angles measured, they are compared with Kang *et al.* [30] (Fig. 7), who measured compensation angles at the centric receiver at

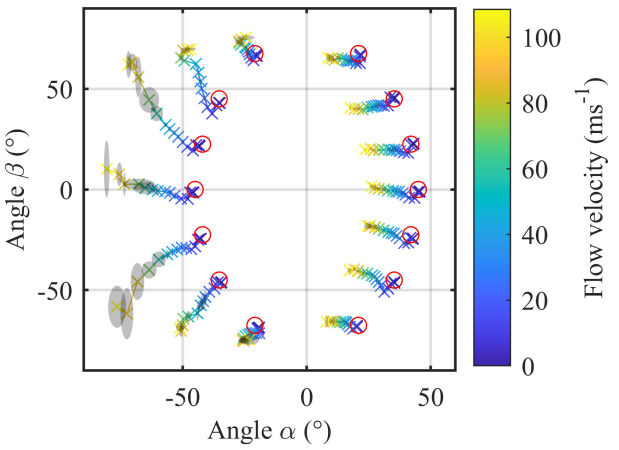

FIGURE 6. The compensation angles are measured for each receiver and each flow rate. The o's are the receiver positions in the fan-shaped path arrangement. On the left are the upstream receivers and on the right are the downstream receivers. The gray ovals are the 95% confidence intervals of the compensation angles.

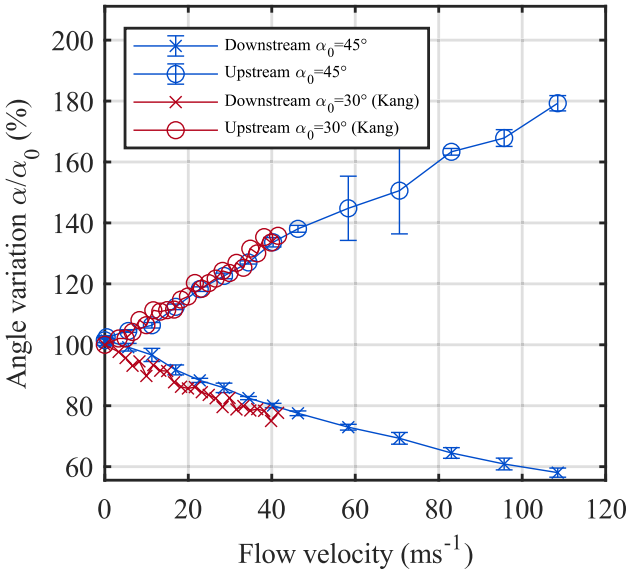

FIGURE 7. The compensation angle for the center receiver measured in this work is compared with the compensation angles measured by Kang *et al.* [30]. Kang *et al.* use a different mechanical inclination angle $\alpha_0 = 30°$ than compared to this work $\alpha_0 = 45°$. However, when considering the percentage angle deviation, the data matches well.

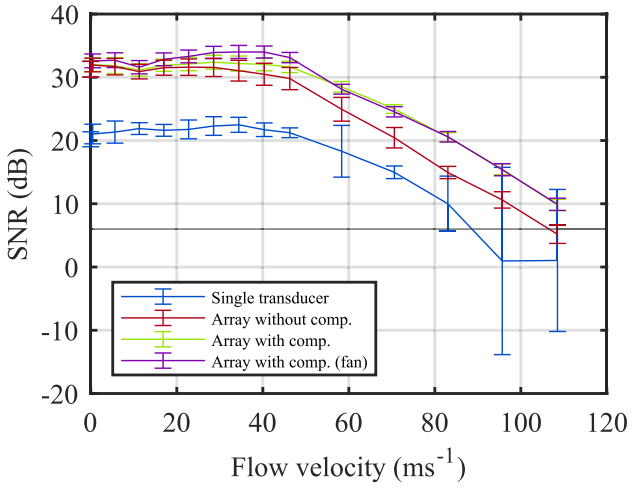

FIGURE 8. The SNR at the $\beta = 0°$ upstream receiver is the lowest absolute SNR for all four measurement methods. We consider the measurements with less SNR than 6 dB (black line) unreliable.

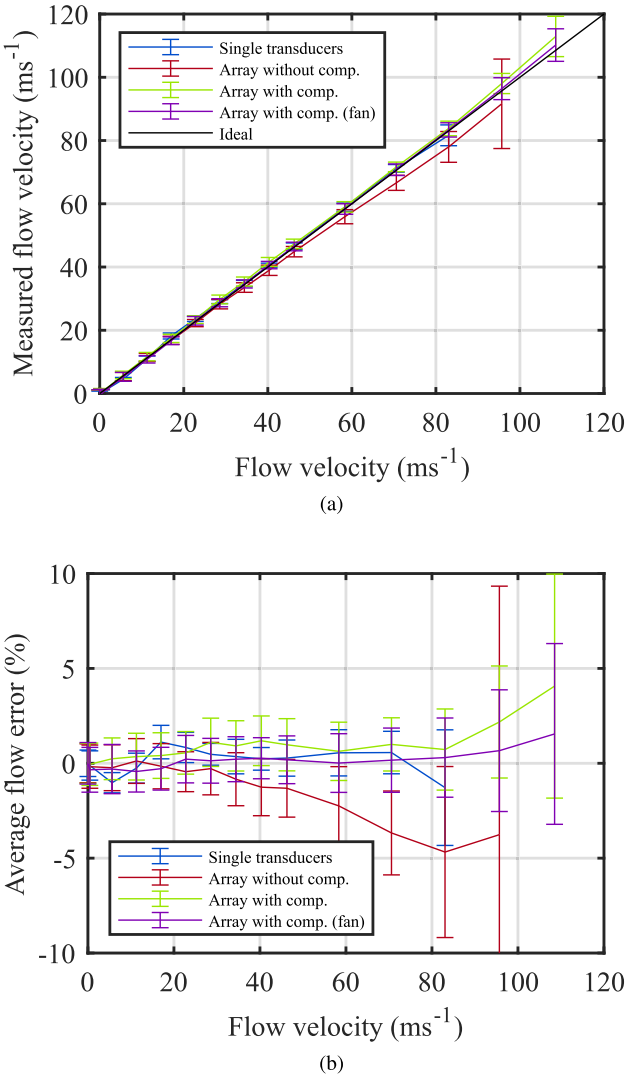

FIGURE 9. The measured flow velocity (a) is close to the reference flow velocity measured with a difference pressure nozzle. The phased-array methods with compensation feature a larger range of measurable flow rates, due to their higher SNR (Fig. 8). The average flow error (b) indicates an offset at all phased-array methods. However, this can be removed by calibration. The error bars are the standard deviations, which increase with decreasing SNR.

flow rates up to 41.5 m s^{-1}. The compensation angles measured by Kang *et al.* have been numerically validated by Choudhary *et al.* [45]. Since Kang *et al.* [30] used different mechanical angles compared to this work, only the percentage angle deviation is available for comparison. Kang *et al.* also use a different pipe diameter, but the compensation angles are independent from the pipe diameter [45]. At 41.5 m s^{-1}, the upstream angle variations deviate by only 3 % and downstream by 5 %. Systematic deviations at the downstream angles are possibly due to a mechanically tilted installation. Nevertheless, the deviations are small, since the angle step size used for compensation angle determination is 3°≙6.6 % in this work. Therefore, our results confirm the findings of Kang *et al.* [30] and go further, as we measured the compensation angle in a higher velocity range up to 107 m s^{-1}, and, additionally for six off-centric receivers.

B. COMPARISON OF THE CONFIGURATIONS

The conventional method with single transducers as transmitters and parallel paths [Fig. 2(a)] is compared to three phased-array based methods: The parallel path with compensation disabled [Fig. 2(b1)], the parallel path with compensation enabled [Fig. 2(b2)], and the fan-shaped path arrangement with compensation enabled [Fig. 2(c)]. In order to compare these, the SNRs (Fig. 8) and the measured flow values (Fig. 9) are used.

Using a phased-array provides 11.1 dB more SNR than using single transducers as transmitters at zero flow. This SNR difference is expectable, as the energy of all 64 transducers in the phased-array add up to an increase of 10 log(64) = 18 dB, when they all constructively interfere with each other. There are about 7 dB losses due to the small openings in the waveguide for each transducer and the impedance mismatch between the waveguide and the free space.

Without compensation, the SNR advantage of the phased-array compared to the single transducers decreases from 11.1 dB to 4.95 dB at 83 m s^{-1}. When the compensation is enabled, the SNR advantage of the phased-array is maintained at higher flow rates (10.6 dB). At a flow velocity of 107 m s^{-1} it is still possible to reliably measure flow with the phased-array. This allows a higher range of measurable flow rates, since we defined a minimum SNR of 6 dB as being required for measurement.

The SNR decrease of the phased-array method without compensation (Fig. 8) compared to the single transducer method can be explained by the narrow sound beam not being aligned to the receiver. This decrease is not observed at the single transmitter, as it has a much smaller aperture

size and a wide sound lobe. When the aperture size of the single transmitter is larger, similar results to the phased-array setup without compensation are expected. The larger aperture leads to more SNR and a more severe sound-drift effect.

The RMS difference between the fan-shaped configurations with compensation enabled and the parallel path configuration with compensation enabled, averaged over all receivers, is only 3 dB. This RMS difference is small compared to an average SNR of 25.8 dB of the fan-shaped configuration. Due to the radial symmetric flow, a significant difference between the parallel and fan-shaped path arrangement was not expected. The fan-shaped arrangement has been previously examined theoretically by Tereshchenko [6]. For radial asymmetric flow the fan-shaped arrangement introduces a systematic error.

In order to calculate the flow velocity, the length of the direct distance between finite-sized transmitter and receiver is required. In the case for which the sound drift effect is not compensated [Fig. 9(a), red], the start and the end of the wave propagation is unknown, resulting in a too short length being used, and, thus, a too low velocity with higher uncertainty being calculated. The array methods with compensation enabled [Fig. 9(a), green and purple] feature a lower error with the remaining deviation being caused by the uncertainty at the receiver side regarding the sound path length.

For industrial applications of a phased-array in a UFM the scanning technique, used in this work, is not feasible due to the large amount of sound bursts to transmit and receive. Instead, it is possible to measure the compensation angles in advance or use theoretical estimations for compensation angles. A more elaborate method is a continuous approach, where each flow measurement adds some information to the compensation angle estimation.

Using a phased-array in a multipath UFM raises the complexity significantly. A different setup using broadband transducers and a more sophisticated signal processing algorithm also has the potential to increase the range of measurable flow rates with a lower complexity by raising the SNR, e.g. with [20]–[22]. However, a more sophisticated narrowband signal processing algorithm is applicable to the phased-array method if the compensation angles are known in advance, e.g. by measuring them as shown in this work.

IV. CONCLUSION AND OUTLOOK

In this paper, we compared three different configurations for using a phased-array in a multipath flow meter with a conventional multipath setup at flow velocities up to 107 $\mathrm{m\,s^{-1}}$. We found that using a phased-array increases the SNR of the measurement compared to a single transmitter arrangement. By compensating the sound-drift effect with the phased-array more SNR is received at high flow velocities. Therefore, we showed that using a phased-array for gas flow measurement in a multipath arrangement leads to an extension of the range of measurable flow rates. Compared to the single transmitter arrangement, a relative accuracy improvement when using a phased-array with compensation enabled was found.

A single phased-array in the fan-shaped arrangement is a viable and cost-effective option, compared to a parallel path setup with multiple arrays. However, the parallel path arrangement is optimal for radial asymmetric flow profiles. Besides that, the phased-array always is recommended to be used with sound drift compensation enabled, since it provides more SNR at high flow rates. As the sound drift effect also occurs orthogonal to the flow, a 2D phased-array is necessary for full compensation.

The phased-array multipath UFM presented is a research platform to evaluate compensation angles for different flow velocities, which will be used as transducer mounting angles. In future, the phased-array method can be used to extend the range of measureable flow rates, particularly when other methods to extend the range of measurable flow rates are not applicable or already applied.

In future work, we will simulate the ideal compensation angles using ray-tracing and compare them to the measurements. Additionally, we will examine further use of these compensation angles as mechanical mounting angles for conventional single transducer multipath UFMs. Another future experiment is adding a second phased-array on the receiver side for increased accuracy.

REFERENCES

[1] L. C. Lynnworth and Y. Liu, "Ultrasonic flowmeters: Half-century progress report, 1955–2005," *Ultrasonics*, vol. 44, Dec. 2006, Art. no. e1371.

[2] G. Rajita and N. Mandal, "Review on transit time ultrasonic flowmeter," in *Proc. 2nd Int. Conf. Control, Instrum., Energy Commun. (CIEC)*, Jan. 2016, pp. 88–92.

[3] L. C. Lynnworth, *Ultrasonic Measurements for Process Control: Theory, Techniques, Applications*. New York, NY, USA: Academic, 1989.

[4] J. Gätke, *Akustische Strömungs-Und Durchflussmessung*. Berlin, Germany: Akad.-Verlag, 1991. [Online]. Available: http://scans.hebis.de/HEBCGI/show.pl?01735423_toc.pdf

[5] Q. Chen, W. Li, and J. Wu, "Realization of a multipath ultrasonic gas flowmeter based on transit-time technique," *Ultrasonics*, vol. 54, no. 1, pp. 285–290, Jan. 2014.

[6] S. A. Tereshchenko and M. N. Rychagov, "Acoustical multipath flow measurements based on quadrature integration methods," *Acoust. Phys.*, vol. 50, no. 1, pp. 100–106, Jan. 2004.

[7] G. Chen, G. Liu, B. Zhu, and W. Tan, "3D isosceles triangular ultrasonic path of transit-time ultrasonic flowmeter: Theoretical design and CFD simulations," *IEEE Sensors J.*, vol. 15, no. 9, pp. 4733–4742, Sep. 2015.

[8] D. Kurniadi, "Transit time multipath ultrasonic flowmeter: An issue on acoustic path arrangement," *Appl. Mech. Mater.*, vol. 771, pp. 3–8, Jul. 2015.

[9] T. Tresch, P. Gruber, and T. Staubli, "Comparison of integration methods for multipath acoustic discharge measurements," in *Proc. IGHEM*, 2006, pp. 1–16.

[10] A. Voser, C. Bruttin, J. E. Prenat, and T. Staubli, "Improving acoustic flow measurement," *Int. Water Power Dam Construct.*, vol. 48, no. 4, pp. 30–34, 1996.

[11] C. N. Pannell, W. A. B. Evans, and D. A. Jackson, "A new integration technique for flowmeters with chordal paths," *Flow Meas. Instrum.*, vol. 1, no. 4, pp. 216–224, 1990.

[12] X. Tang, Q. Yang, and Y. Sun, "Gas flow-rate measurement using a transit-time multi-path ultrasonic flow meter based on PSO-SVM," in *Proc. IEEE Int. Instrum. Meas. Technol. Conf. (I2MTC)*, May 2017, pp. 1–6.

[13] T. Tresch, B. Lüscher, T. Staubli, and P. Gruber, "Presentation of optimized integration methods and weighting corrections for the acoustic discharge measurement," in *Proc. Int. Conf. Hydraulic Efficiency Meas.*, 2008, pp. 1–14.
[14] L. Fei, H. Cunfu, W. Bin, and J. Jingpin, "Numerical simulation of multi-path ultrasonic flowmeter: Ultrasonic path error analysis," in *Proc. 1st Int. Conf. Sensor Device Technol. Appl.*, Jul. 2010, pp. 58–62.
[15] M. Orvatinia, "Improvement of accuracy in multi-path ultrasonic flow meters," *Sensors Transducers*, vol. 231, no. 3, pp. 1–9, 2019.
[16] X. Tang, X. Xie, H. Zhang, and H. Zhou, "Data integration for multi-path ultrasonic flowmeter based on Levenberg–Marquardt algorithm," *IET Sci. Meas. Technol.*, vol. 9, no. 8, pp. 909–920, 2015.
[17] D. Zheng, D. Zhao, and J. Mei, "Improved numerical integration method for flowrate of ultrasonic flowmeter based on Gauss quadrature for non-ideal flow fields," *Flow Meas. Instrum.*, vol. 41, pp. 28–35, Mar. 2015.
[18] H. Zhao, L. Peng, T. Takahashi, T. Hayashi, K. Shimizu, and T. Yamamoto, "ANN based data integration for multi-path ultrasonic flowmeter," *IEEE Sensors J.*, vol. 14, no. 2, pp. 362–370, Feb. 2014.
[19] L. Hu, L. H. Qin, K. Mao, W. Y. Chen, and X. Fu, "Optimization of neural network by genetic algorithm for flowrate determination in multipath ultrasonic gas flowmeter," *IEEE Sensors J.*, vol. 16, no. 3, pp. 1158–1167, Mar. 2016.
[20] D. M. Van Willigen, P. L. Van Neer, J. Massaad, N. De Jong, M. D. Verweij, and M. A. Pertijs, "An algorithm to minimize the zero-flow error in transit-time ultrasonic flow meters," *IEEE Trans. Instrum. Meas.*, vol. 70, 2020, Art. no. 7500109.
[21] F. Sunol, D. A. Ochoa, and J. E. Garcia, "High-precision time-of-flight determination algorithm for ultrasonic flow measurement," *IEEE Trans. Instrum. Meas.*, vol. 68, no. 8, pp. 2724–2732, Aug. 2019.
[22] Z. Fang, L. Hu, L. Qin, K. Mao, W. Chen, and X. Fu, "Estimation of ultrasonic signal onset for flow measurement," *Flow Meas. Instrum.*, vol. 55, pp. 1–12, Jun. 2017.
[23] M. Kupnik, A. Schroder, and M. Groschl, "PS-16 adaptive asymmetric double-path ultrasonic transit-time gas flowmeter," in *Proc. IEEE Ultrason. Symp.*, Oct. 2006, pp. 2429–2432.
[24] K. S. Mylvaganam, "High-rangeability ultrasonic gas flowmeter for monitoring flare gas," *IEEE Trans. Ultrason., Ferroelectr., Freq. Control*, vol. 36, no. 2, pp. 144–149, Mar. 1989.
[25] F. C. Lowell and R. H. Lyon, "Method and apparatus for measuring flow by using phase advance," U.S. Patent 5 228 347, Jul. 20, 1993.
[26] J. S. Hall, "Perpendicular fluid flow measurement with a spatial array of ultrasonic transducers," in *Proc. IEEE Int. Ultrason. Symp.*, Sep. 2009, pp. 741–744.
[27] L. Kang *et al.*, "Flow velocity measurement using a spatial averaging method with two-dimensional flexural ultrasonic array technology," *Sensors*, vol. 19, no. 21, p. 4786, Nov. 2019.
[28] A. Jager *et al.*, "Air-coupled 40-kHz ultrasonic 2D-phased array based on a 3D-printed waveguide structure," in *Proc. IEEE Int. Ultrason. Symp. (IUS)*, Sep. 2017, pp. 1–4.
[29] H. Daßler, L. Thieme, and W. Manthey, "Broadband ultrasonic MEMS for liquids," in *Proc. 16th IMEKO World Congr.*, vol. 2, 2000, pp. 343–347.
[30] L. Kang *et al.*, "Two-dimensional flexural ultrasonic phased array for flow measurement," in *Proc. IEEE Int. Ultrason. Symp. (IUS)*, Sep. 2017, pp. 1–4.
[31] A. Jager *et al.*, "Ultrasonic phased array for sound drift compensation in gas flow metering," in *Proc. IEEE Int. Ultrason. Symp. (IUS)*, Sep. 2017, pp. 1–4.
[32] C. Haugwitz *et al.*, "Flow metering of gases using ultrasonic phased-arrays at high velocities," in *Proc. IEEE Int. Ultrason. Symp. (IUS)*, Oct. 2019, pp. 1129–1132.
[33] *Fans—Performance Testing Using Standardized Airways*, document ISO 5801:2017(E), Sep. 2017.
[34] *Measurement of Fluid Flow by Means of Pressure Differential Devices Inserted in Circular Cross-Section Conduits Running Full—Part 3: Nozzles and Venturi Nozzles*, document ISO 5167-3:2003, Jan. 2004.
[35] S. S. Crump, "Modeling apparatus for three-dimensional objects," U.S. Patent 5 340 433, Aug. 23, 1994.
[36] A. Kak and M. Slaney, *Principles of Computerized Tomographic Imaging*. Philadelphia, PA, USA: SIAM, 2001, ch. 3.
[37] A. H. Khan and R. A. Chaudhuri, "Fan-beam geometry based inversion algorithm in computed tomography (CT) for imaging of composite materials," *Composite Struct.*, vol. 110, pp. 297–304, Apr. 2014.
[38] U. Kruse, "Experimental investigation of a centrifugal fan to the influence of the Mach number effect," M.S. thesis, Chair Fluid Syst., Technische Universität Darmstadt, Darmstadt, Germany, 2015.
[39] M. Kupnik, E. Krasser, and M. Groschl, "3D-1 absolute transit time detection for ultrasonic gas flowmeters based on time and phase domain characteristics," in *Proc. IEEE Ultrason. Symp.*, Oct. 2007, pp. 142–145.
[40] D. Van Willigen, P. Van Neer, J. Massaad, M. Verweij, N. De Jong, and M. Pertijs, "Minimizing the zero-flow error in transit-time ultrasonic flow meters," in *Proc. IEEE Int. Ultrason. Symp. (IUS)*, Oct. 2018, pp. 1–4.
[41] M. Rutsch *et al.*, "Waveguide for air-coupled ultrasonic phased-arrays with propagation time compensation and plug-in assembly," *J. Acoust. Soc. Amer.*, vol. 150, no. 5, pp. 3228–3237, Nov. 2021.
[42] G. Allevato *et al.*, "Real-time 3-D imaging using an air-coupled ultrasonic phased-array," *IEEE Trans. Ultrason., Ferroelectr., Freq. Control*, vol. 68, no. 3, pp. 796–806, Mar. 2021.
[43] L.-B. Mu, K.-J. Xu, B. Liu, L. Tian, and L.-P. Liang, "Echo signal envelope fitting based signal processing methods for ultrasonic gas flow-meter," *ISA Trans.*, vol. 89, pp. 233–244, Jun. 2019.
[44] A. D. Pierce, *Acoustics: An Introduction to its Physical Principles and Applications*. Cham, Switzerland: Springer, 2019, Ch. 8.
[45] K. P. Choudhary, V. Arumuru, and Y. G. Bhumkar, "Numerical simulation of beam drift effect in ultrasonic flow-meter," *Measurement*, vol. 146, pp. 705–717, Nov. 2019.

CHRISTOPH HAUGWITZ (Student Member, IEEE) received the M.Sc. degree in electrical engineering from the Technische Universität Darmstadt, Germany, in 2021. Since then, he has been a Research Associate with the Measurement and Sensor Technology Group, TU Darmstadt. His research interests include ultrasonic flow metering, air-coupled ultrasonic phased-arrays, and its applications.

CLAAS HARTMANN (Graduate Student Member, IEEE) received the M.Sc. degree in electrical engineering from Technische Universität Darmstadt, Germany, in 2018. Since 2018, he has been a Research Associate with the Measurement and Sensor Technology Group, TU Darmstadt. His research interests include structurally integrated mechanical sensors and additive manufacturing of sensors, volume, and mass flow rate sensor tests and calibrations.

GIANNI ALLEVATO (Student Member, IEEE) received the M.Sc. degree in electrical engineering from Technische Universtität Darmstadt, Germany, in 2018. Since 2018, he has been a Research Associate with the Measurement and Sensor Technology Group, TU Darmstadt. His research interests include electronics and embedded systems design, software development, and parallel signal processing for imaging with air-coupled ultrasonic phased-arrays and its applications.

MATTHIAS RUTSCH (Graduate Student Member, IEEE) received the B.Sc. degree from Brandenburgische Technische Universität Cottbus, Germany, in 2014, and the M.Sc. degree in electrical engineering from Technische Universität Darmstadt in 2017. Since then, he has been a Research Associate at the Measurement and Sensor Technology Group, Technische Universität Darmstadt. His research interests include simulation and characterization of duct acoustics for air-coupled ultrasound applications.

JAN HINRICHS (Graduate Student Member, IEEE) received the M.Sc. degree in electrical engineering from Technische Universität Darmstadt, Germany, in 2017. Since then, he has been a Research Associate with the Measurement and Sensor Technology Group, TU Darmstadt. His research interests include sensor design, sensor electronics, acoustoelastic sensing, and nondestructive examination using Lamb waves.

JOHANNES BRÖTZ received the M.Sc. degree in mechanical engineering from Technische Universität Darmstadt, Germany, in 2018. Since 2018, he has been a Research Associate with the Chair of Fluid Systems, TU Darmstadt. His research interests include loss modeling in turbomachinery, aerodynamics, and experimental validation.

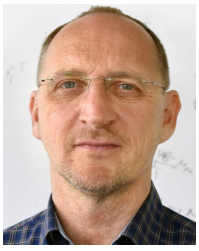

DIETER BOTHE received the Diploma degree in mathematics, the Ph.D. degree in mathematics, and the Habilitation degree in mathematics from the University of Paderborn, Germany, in 1988, 1993, and 2000, respectively. From 1999 to 2005, he headed the Modelling, Analysis and Simulation of Multiphase Flows Group, Chemical Engineering Institute, University of Paderborn. From 2005 to 2009, he was the Chair for Mathematics/CCES, RWTH Aachen, Germany. Since 2009, he has been a Full Professor at TU Darmstadt, Germany, where he is currently the Head of the Mathematical Modeling and Analysis Group. His research topics are mathematical modeling, numerical simulation, and analysis of two-phase flows with transport processes at fluid interfaces, multicomponent diffusion, mass transfer with chemical reactions, surfactant influence, and Non-Newtonian flow.

PETER F. PELZ received the Diplom-Ingenieur degree in mechanical engineering from Technische Universität Darmstadt, Darmstadt, Germany, in 1993, and the Dr.-Ing. degree in mechanical engineering from Technische Universität Darmstadt, under Prof. Dr.-Ing. Joseph H. Spurk. After his Diplom-Ingenieur degree, he continued working with Technische Universität Darmstadt as a Research Assistant. From 1998 to 2003, he worked as the Team Leader of Fluid Mechanics and Rheology at Freudenberg F&D Service KG, Weinheim, followed by the position as the Manager of Advanced Development at Vibracoustic GmbH and Co KG, Hamburg, from 2003 to 2006. Since 2006, he has been a Full Professor at Technische Universität Darmstadt, where he is the Head of the Chair of Fluid Systems (FST). His research topics are sustainable systems design, urbanization and infrastructures, cavitation and generic flows, and designing with fluids. He has been a Spokesperson of the Collaborative Research Centre (SFB) 805 on uncertainty in mechanical engineering and is one of the initiators and the Deputy Spokesperson of the National Research Data Infrastructure for Engineering Sciences NFDI4Ing. During his research time, he co-founded the Industrial Science GmbH, Darmstadt, where he currently is a Key-Researcher.

MARIO KUPNIK (Senior Member, IEEE) received the Diplom-Ingenieur degree in electrical engineering from the Graz University of Technology, Graz, Austria, in 2000, and the Ph.D. degree in electrical engineering from the University of Leoben, Leoben, Austria, in 2004. From 2005 to 2011, he was working as a Post-Doctoral Researcher, a Research Associate, and a Senior Research Scientist at the Edward L. Ginzton Laboratory, Stanford University, Stanford, CA, USA. From 2011 to 2014, he was a Full Professor of electrical engineering at the Brandenburg University of Technology, Cottbus, Germany. Since 2015, he has been a Full Professor at Technische Universität Darmstadt, Darmstadt, Germany, where he is currently the Head of the Measurement and Sensor Technology Group. His research topics are micromachined sensors and actuators, multiphysics simulations, flowmetering of gases and liquids, ultrasound, electroacoustics, and harsh-environment instrumentation.